Ocean Engineering 76 (2014) 32–39

Contents lists available at ScienceDirect

Ocean Engineering

journal homepage: www.elsevier.com/locate/oceaneng

Modelling of seismic airgun bubble dynamics and pressure field using the Gilmore equation with additional damping factors

K.L. de Graaf*, I. Penesis, P.A. Brandner

Australian Maritime College, University of Tasmania, Tasmania 7250, Australia

ARTICLE INFO

Article history:
Received 7 January 2013
Accepted 1 December 2013
Available online 18 December 2013

Keywords:
Seismic airgun
Gilmore equation

ABSTRACT

Seismic airguns are commonly used in geophysical exploration. More recently, they are also being used as an alternative to underwater explosions for the shock testing of defence vessels. The study of the dynamics of the bubble produced by a seismic airgun is beneficial in understanding the resultant pressure field and shockwave. The Rayleigh–Plesset and Gilmore equations for modelling spherical bubble dynamics are compared for the expansion of an initially highly pressurised gas bubble. The relationship between initial gas pressure and both the first maximum bubble radius and the first period of oscillation are presented. The separate contributions due to the presence of the airgun body, mass throttling, effective viscosity and heat diffusion to the first maximum radius and period are modelled and discussed. The effects of evaporation and condensation at the bubble wall are also considered. Gilmore's model is used to predict the radiated pressure wave of the new bubble model. The results are in fair agreement with measured data collected from full scale airgun trials.

© 2013 Elsevier Ltd. All rights reserved.

1. Introduction

The Royal Australian Navy is currently investigating the feasibility and advantages of employing seismic airguns for shock testing naval craft. Shock testing with seismic airguns, rather than high explosives, is less expensive, safer, and more environmentally friendly. To perform shock testing effectively, an array of airguns must be used and the interactions between the bubbles can alter the pressure fields produced. Several methods exist for calculating the interactions between highly nonlinear airgun bubbles in an array (Laws et al., 1990; Vaage and Ursin, 1987), but all rely on a basic understanding of the parameters affecting a single airgun bubble and the pressure field and shockwave produced.

The underlying principle of an airgun relies on a firing chamber, filled with compressed gas, which is held shut via a pressure difference across the two ends of a shuttle. The lower flange of the shuttle in Fig. 1a is larger than the upper flange. When the pressure difference across one end of the shuttle (in this case, the lower flange) is equalised (Fig. 1b), the shuttle can open and the compressed air in the firing chamber exhausts through several 'ports' in the body of the airgun, and forms the bubble. The gun is usually reset through the use of a second chamber of air–not shown here.

The Gilmore equation for bubble dynamics is commonly used as the underlying basis for seismic airgun bubbles and underwater explosions. Comparisons of this equation with other bubble models, including the well known Rayleigh–Plesset equation, exist; however, they consider a bubble's collapse from its maximum radius rather than expansion from its minimum radius. In modelling seismic airgun bubbles, it is more practical to consider the initial bubble pressure and radius, rather than the conditions at the first maximum. The present work compares the Gilmore equation to the Rayleigh–Plesset equation to confirm the use of the Gilmore equation as the basic bubble model.

Several contributions have been made to improve the numerical modelling of individual seismic airgun bubbles by considering additional factors to the basic bubble dynamics. Ziolkowski (1970) used Gilmore's equation and found a polytropic index of 1.13 gave good results for the first period of oscillation; this value was also obtained by Dragoset (1984) for a range of gun sizes. Schulze-Gattermann (1972) emphasised the effect of the actual airgun body on the period of oscillation. Safar (1976) compared the equation of a bubble to an electrical circuit and developed a model for the rise time, amplitude of the initial pulse, and period of the airgun. Johnston (1982) and Dragoset (1984) considered the effect of the shuttle motion and choked flow rate on the chamber pressure, with Dragoset allowing for the actual port size. Ziolkowski (1982) proposed that heat transfer occurs through the latent heat absorbed and released by evaporation and condensation at the bubble wall. This concept is repeated by Langhammer and Landrø (1993). Laws et al. (1990) consider mass transfer due to evaporation and condensation,

* Corresponding author. Tel.: +61 6324 9723; fax: +61 6324 9592.
E-mail address: kdegraaf@amc.edu.au (K.L. de Graaf).

0029-8018/$ - see front matter © 2013 Elsevier Ltd. All rights reserved.
http://dx.doi.org/10.1016/j.oceaneng.2013.12.001

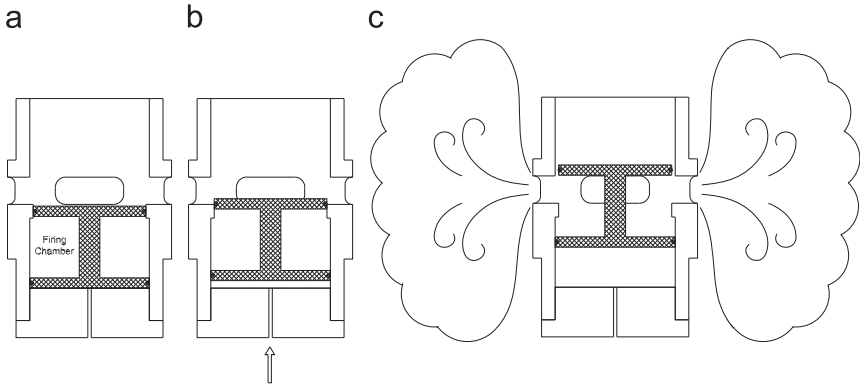


Fig. 1. Illustration of airgun firing in three stages: (a) pressurised chamber under equilibrium, (b) equalisation of pressure across lower flange to fire shuttle and (c) release of air through ports to form bubble.

conductive heat diffusion, flow throttling and an 'effective viscosity' induced by the turbulent nature of the bubble. It is claimed that this turbulent nature also has an amplifying effect on the heat transfer across the bubble wall. Li et al. (2010) include the effect of mass throttling (but not choked flow) through ports, the airgun body, heat transfer and hydrostatic pressure changes as the bubble rises through the water.

There appears to be no work that considers all of these parameters together and provides values for coefficients with a summary of the impact of each parameter on the bubble behaviour. In this work, the Gilmore equation is used as the basic bubble model and the individual and combined effects of the presence of the airgun body, mass throttling, effective viscosity, heat diffusion and condensation and evaporation are considered. Preliminary results using this approach have been presented by de Graaf et al. (2012). The present work provides more detailed results, including a prediction of the radiated pressure wave using Gilmore's theory, and makes comparison with experimental data.

2. Comparison of Rayleigh–Plesset and Gilmore equations

The Rayleigh–Plesset equation describes the motion of a spherical bubble in an incompressible liquid (Franc and Michel, 2004). When considering bubble velocities of an appreciable order of magnitude compared with the speed of sound in water, compressibility of the liquid cannot be ignored. The Gilmore equation includes second-order compressibility terms, accounting for the loss of bubble energy due to the radiated acoustic and pressure waves (Gilmore, 1952). Both equations are commonly used to model bubble dynamics, with the Gilmore equation often used in underwater explosion applications. The Rayleigh–Plesset equation is given by

$$\rho\left[R\ddot{R}+\frac{3}{2}\dot{R}^2\right]=p_0\left(\frac{R_0}{R}\right)^{3k}+p_v-\frac{2S}{R}-4\mu\frac{\dot{R}}{R}-p_\infty \tag{1}$$

where ρ is the water density, R is the bubble radius, p_0 is the initial non-condensable gas pressure, R_0 is the initial bubble radius, k is the polytropic index, which varies between 1 (isothermal) and 1.4 (adiabatic)—taken as 1.4 in this work where required, p_v is the vapour pressure, S is the surface tension, μ is the dynamic viscosity and p_∞ is the ambient water pressure. Overdots represent differentiation with respect to time.

The Gilmore equation is given by

$$R\ddot{R}\left(1-\frac{\dot{R}}{c}\right)+\frac{3}{2}\dot{R}^2\left(1-\frac{\dot{R}}{3c}\right)=H\left(1+\frac{\dot{R}}{c}\right)+\frac{R\dot{H}}{c}\left(1-\frac{\dot{R}}{c}\right) \tag{2}$$

where the enthalpy difference, H, is defined as $\int_{p_\infty}^{p} \mathrm{d}p/\rho$ and c is the local speed of sound. Gilmore (1952) uses the Tait equation of state to define H as a function of c and p, giving

$$H=n\left(\frac{p_\infty+B}{(n-1)\rho}\right)\left[\left(\frac{p+B}{p_\infty+B}\right)^{n-1/n}-1\right] \tag{3}$$

$$c=c_\infty\left[\left(\frac{p+B}{p_\infty+B}\right)^{n-1/2n}\right] \tag{4}$$

$$p=p_0\left(\frac{R_0}{R}\right)^{3k}+p_v-\frac{2S}{R}-4\mu\frac{\dot{R}}{R} \tag{5}$$

$$c_\infty=\sqrt{n\left(\frac{p_\infty+B}{\rho}\right)} \tag{6}$$

where c_∞ represents the speed of sound at an infinite distance from the bubble, and B and n are constants. Gilmore (1952) gives $B=3000$ atm and $n=7$.

The equations are solved using the classical fourth-order Runge–Kutta method. An adaptive time-step is often used for modelling dynamics of vapour filled bubbles due to the nearly infinitely high interface velocities that develop during the collapse. The bubbles considered here have a large non-condensable gas content which arrests the bubble collapse and limits the bubble wall velocities achieved. Adaptive time-stepping can also be required for smaller bubbles for which the contributions of terms such as surface tension and dynamic viscosity are significant, increasing the number of parameters in the solution, and resulting in extremely stiff nonlinear equations.

Vokurka (1986) compared these two equations for bubble collapse and determined that for amplitudes ($R_{max}/R_{equilibrium}$) greater than 2, the Gilmore equation produces superior results. Other comparisons made between these equations also model the bubble collapse assuming the bubble starts at its maximum radius and lowest pressure—representative of a newly formed cavitation bubble. In these comparisons, the collapse of a Gilmore bubble is fractionally (1.005) longer than the collapse of a Rayleigh bubble (Franc and Michel, 2004).

This work compares the Rayleigh–Plesset and Gilmore equations with the bubble initially at its smallest radius and highest pressure—as would be more appropriate when considering seismic airguns and underwater explosions. For both equations, the first maximum radius as a function of the initial pressure for the expanding bubbles is shown (Fig. 2). The maximum radius and initial pressure have been non-dimensionalised with respect to initial bubble radius and ambient water pressure respectively.

When modelling a bubble initially at its minimum point through one expansion and collapse cycle, a smaller maximum bubble radius is predicted by the Gilmore equation, which leads to

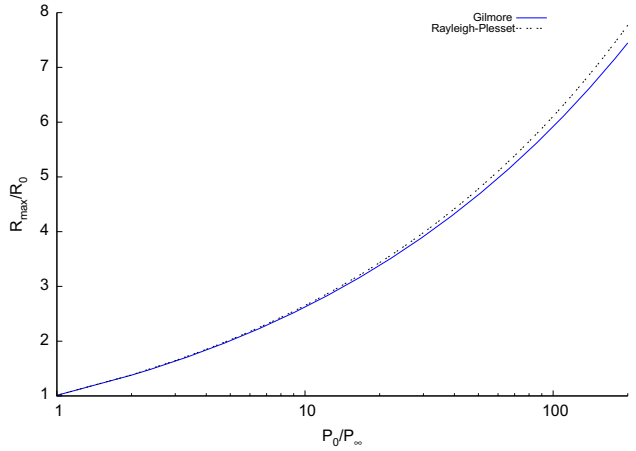


Fig. 2. First maximum radius as a function of initial pressure predicted by Rayleigh–Plesset and Gilmore equations with initial radius of 0.1 m.

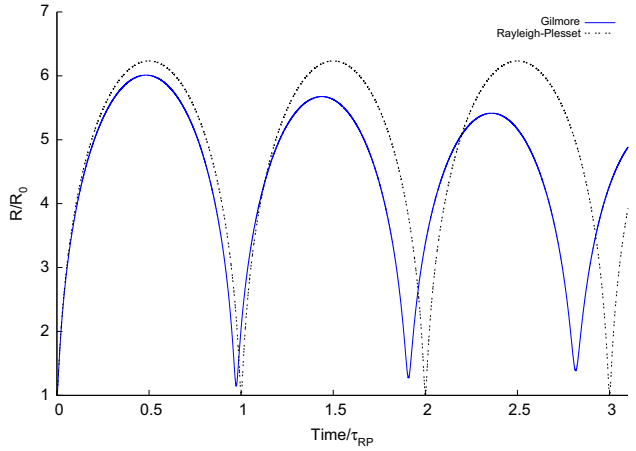


Fig. 3. Comparison of predicted temporal variation and maximum non-dimensional bubble radii from Rayleigh–Plesset and Gilmore equations for an initial pressure and radius of 100 bar and 0.1 m respectively. τ_{RP} is the collapse time for the Rayleigh–Plesset bubble.

a shorter period when compared with the Rayleigh–Plesset solution (Fig. 3).

This study compares the Rayleigh–Plesset and Gilmore equations for use in modelling seismic airgun or underwater explosion type bubbles (initially at a minimum radius and maximum pressure) in contrast to modelling cavitation type bubbles (initially at maximum radius and minimum pressure)—the latter being the commonly published study. Further study shows that the surface tension and dynamic viscosity terms are negligible in both solutions due to the size of these explosion type bubbles. Noticeable damping from these two terms is evident in bubbles with an initial radius in the order of 100 μm. The equivalent initial radius of a full-scale airgun is in the order of 10–100 mm. Removal of these terms reduces the Rayleigh–Plesset equation to what is known as simply the Rayleigh equation.

Fig. 2 illustrates the increasing disparity between the two equations with increasing initial pressure. For seismic airguns, the initial pressure is generally at least an order of magnitude greater than the ambient water pressure, resulting in noticeably different solutions between the Gilmore and Rayleigh equations. The difference in first maximum radius is a function of the compressibility of the water, and the difference in the maximum radii of the subsequent bubble pulses increases with time due to the higher-order terms in the Gilmore equation that account for increased damping due to radiated pressure waves through the compressible liquid (Fig. 3). Results obtained using the Flynn equation (Flynn, 1975), which incorporates the effect of compressibility into the Rayleigh-Plesset equation by means of a constant speed of sound value, are not significantly different from the results obtained from the Gilmore model. This indicates the importance of the acoustic radiation in the bubble damping, and not necessarily the presence of a shock wave. Due to the popularity of the Gilmore equation for modelling underwater explosions, the Gilmore model is the subject of this paper and will be used as the base model for all further predictions. As surface tension is negligible for the size bubble considered here, it will be ignored; however, a dynamic viscosity term is required when calculating the effective viscosity and the thermal boundary layer, and will be included in all simulations for consistency and taken as 1×10^{-3} kg/ms.

3. Additional aspects to the Gilmore equation

It is well noted (Laws et al., 1990; Schulze-Gattermann, 1972; Ziolkowski, 1982; Li et al., 2010) that while the Gilmore equation models compressibility which leads to acoustic damping, additional damping parameters must also be present in the dynamics of an airgun bubble. Typically, a real airgun bubble will have lost its energy after only a few growth/collapse cycles. Predictions with the Gilmore equation result in oscillations that persist much longer. The additional factors identified here have been modelled using the parameters corresponding to Firing A of the experimental data; the initial bubble radius is taken as 0.127 m, the initial pressure is 138 bar and ambient water pressure is 1.29 bar.

To allow the incorporation of terms for mass throttling and temperature effects, the ideal gas law pressure equation (5) is replaced by

$$p=\frac{mR_GT}{V}+p_v \tag{7}$$

where m is the bubble gas mass, R_G is the gas constant, T is the bubble temperature and V is the bubble volume.

When the gun is fired, the air expands through four 'ports' into the surrounding water. Depending on the gun design, the air may also pass through other internal constrictions before release. These orifices throttle the flow rate and considering the pressure differences involved, choked flow conditions can be assumed. The mass flow function is (White, 2003)

$$\dot{m}=A\sqrt{\frac{p_Gm_G}{V_G}\frac{2k}{k-1}\left[\left(\frac{p}{p_G}\right)^{2/k}-\left(\frac{p}{p_G}\right)^{(k+1)/k}\right]} \tag{8}$$

where p is limited to the sonic value, p_G^*:

$$p_G^*=p_G\left(\frac{2}{k+1}\right)^{k/(k-1)} \tag{9}$$

A is the orifice area, in this model taken as 0.0128 m^2, and the subscript G indicates the value inside the airgun chamber. The mass throttling limits the initial maximum radius, subsequently reducing the pressure difference across the bubble wall and the intensity of the following bubble pulses. The reduced initial maximum radius also results in a comparatively shorter first period (Fig. 4). Depending on the design of the airgun, and the method used for resetting the shuttle, the shuttle may close before all the air has been released from the chamber. This effectively decreases the chosen firing volume used in the calculation. In this work, the full firing volume given has been used.

The presence of the airgun body at the bubble centre has been identified as a contributing factor to the bubble dynamics

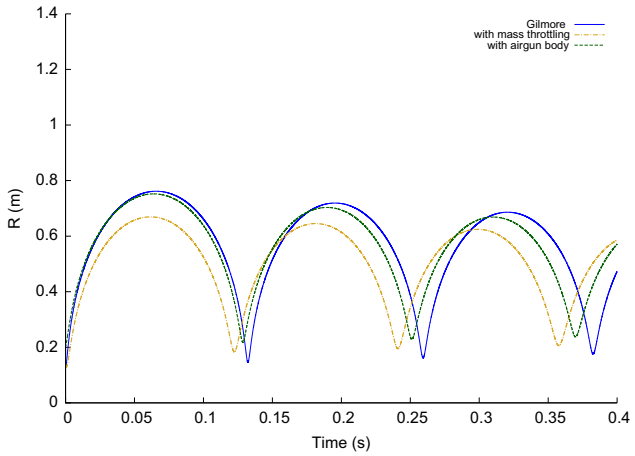


Fig. 4. The effect of including mass throttling and the presence of the airgun body on the solution of the Gilmore equation.

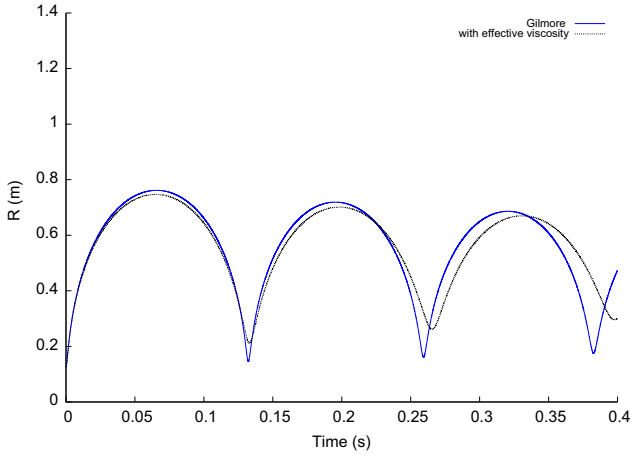


Fig. 5. The effect of including effective viscosity on the solution of the Gilmore equation.

(Schulze-Gattermann, 1972). The volume of air in the bubble is:

$$V = \frac{4}{3}\pi R^3 - V_{AG} \tag{10}$$

where V_{AG} is the volume of the airgun body, in this model taken as 0.027 m^3. This volume is then used to calculate the bubble pressure, which in effect is increased at the maximum bubble radius as compared with the bubble pressure where no body is present. The reduced pressure difference between the bubble and the water reduces the intensity and velocities of the collapse; therefore, the first bubble minimum is larger, and the following oscillations less intense (Fig. 4).

Laws et al. (1990) include an effective viscosity, μ_{eff}, to account for turbulent motion at the bubble wall which occurs at large Reynolds numbers. This increases the heat transfer across the bubble wall and the damping of the bubble oscillation due to turbulent shear stress.

$$\mu_{eff} = \mu(1 + KRe). \tag{11}$$

K is a constant, about 0.02. The Reynolds number, Re, is calculated based on the instantaneous bubble radius and velocity. The effect of increasing the viscosity has a small impact on the damping of the bubble (Fig. 5). Note, the implementation of effective viscosity here considers only the increased damping, and not the increased heat transfer across the bubble wall.

Li et al. (2010) identified that Ziolkowski's (1970) model (essentially Gilmore's model with k equal to 1.13) results in an equilibrium temperature well below that of the surrounding water. The inclusion of heat transfer in the model results in more realistic predictions of equilibrium temperatures. Laws et al. (1990) give the thickness of the thermal boundary layer as

$$d = 4DRe^{-3/4}Pr^{-1/2} \tag{12}$$

where D is the bubble diameter and Pr is the Prandtl number. The rate of heat conduction across this layer is

$$\dot{Q} = \Delta T A \frac{\kappa}{d} \tag{13}$$

where ΔT is the difference in temperature across the bubble wall, A is the surface area of the bubble and κ is the thermal conductivity of the interface. Ni et al. (2011) studied a range of κ/d values from 2000 to 8000 W/m^2K and found correspondence with specific experimental data for a value of 4000 W/m^2K. Herring (1949) states that the flow of heat outward is a function of the thermal conductivity of the gas. The thermal boundary layer will extend across the bubble interface, complicating the value of the thermal conductivity. Here, values for κ of 0.6 W/mK for water and 0.024 W/mK for air have been considered; d is updated through the calculations but is in the order of 100 μm. Due to turbulence, the area across which heat is conducted may be magnified—Laws et al. (1990) used a factor of 10; however, in this example, the actual surface area is used.

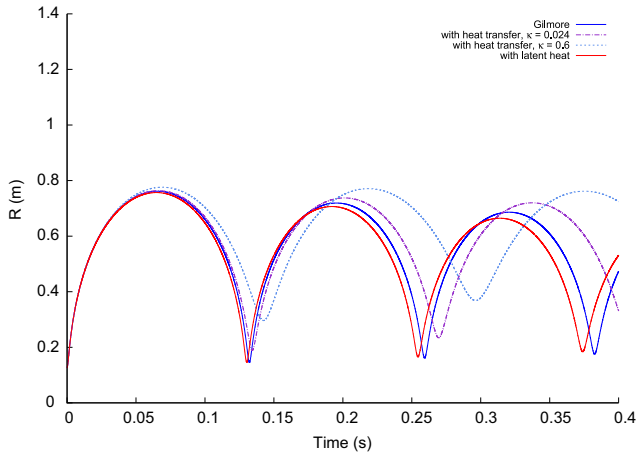


Fig. 6. The effect of including conductive heat transfer and heat transfer through latent heat on the solution of the Gilmore equation.

For underwater explosions and spark- or laser-generated bubbles, the initial minimum bubble is hot and on expansion proceeds to be additionally cooled by the surrounding water. Conversely, the initial airgun bubble is assumed to be at ambient water temperature and as the bubble expands the drop in temperature is lessened by the surrounding water, allowing the bubble to reach a greater maximum radius. The following temperature increase upon collapse is also lessened by the heat transfer, arresting the collapse at a larger minimum radius. The magnitude of the following oscillations is likewise diminished (Fig. 6). The bubble period is increased as a result of the larger maximum bubble radius and reduced velocity of the bubble motion. The variation of the bubble temperature with time is shown in Fig. 7.

In place of conductive heat transfer, Ziolkowski (1982) proposed that the heat transfer takes place through latent heat absorbed/released by evaporation and condensation at the bubble wall. Fujikawa and Akamatsu (1980) produced a detailed mathematical formulation to consider these effects and found that evaporation and condensation strongly influence microbubble dynamics. Simpler models have been used by Laws et al. (1990)

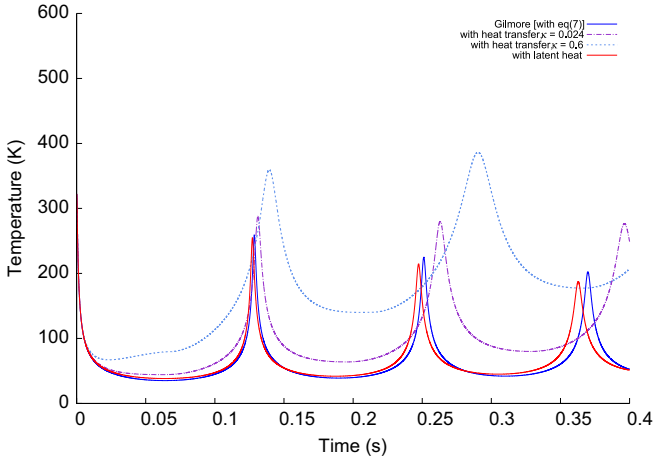


Fig. 7. The effect of including conductive heat transfer and heat transfer through latent heat on the temperature predicted by the Gilmore equation.

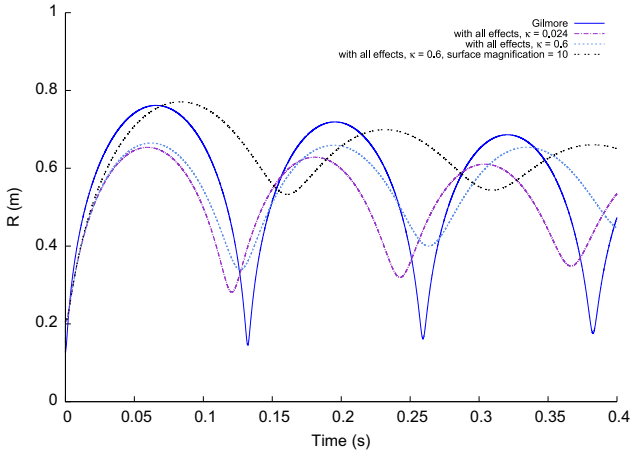


Fig. 8. The combined effect of including all additional factors on the solution to the Gilmore equation.

and Cook et al. (1997). The vapour mass transfer given by Fuijkawa and Akamatsu is

$$\dot{m}_v = \frac{\alpha_M A}{\sqrt{2\pi R_G}}\left[\frac{p_v^*}{\sqrt{T_w}} - \Gamma\frac{p_v}{\sqrt{T}}\right] \tag{14}$$

where α_M is the ratio of vapour molecules sticking to the phase interface and those impinging on it, about 0.04 (Fujikawa and Akamatsu, 1980), A is the surface area of the bubble, p_v^* is the equilibrium vapour pressure (Fujikawa and Akamatsu, 1980) and T_w is the temperature of the water. Γ is a correction factor, assumed to be 1 for these calculations. The heat flow due to the vapour mass transfer is given by

$$\dot{Q} = \dot{m}_v L \tag{15}$$

where L is the latent heat of vaporisation, taken as 2.45 J/kg. The impact on the bubble wall dynamics due to movement of the bubble wall as a result of mass flow has been ignored, as the additional terms are assumed negligible (Cook et al., 1997). Only the effect on bubble temperature and pressure has been considered. Modelling the temperature change due to evaporation and condensation has no appreciable difference on the final bubble temperature, and the mean temperature remains cooler than the surrounding water (Fig. 7). There is little impact on the maximum radius and period of the bubble pulses (Fig. 6). The results here differ from those of Fujikawa and Akamatsu (1980); however, this may be attributed to the difference in size of the initial bubble radius.

Fig. 8 presents the results of including all additional factors discussed here. Solutions have been calculated for both proposed limits of κ with no increase in surface area (i.e. magnification factor of 1). Increasing the surface area in (13) further increases the bubble period and damping. A surface magnification factor of 10 is shown with κ equal to 0.6 W/mK. The resultant bubble period corresponds well with the experimental waveform period (Fig. 10a).

The additional aspects considered in this work have varying effect on the bubble radius and period predicted by the Gilmore equation. The inclusion of conductive heat transfer in the model has the single greatest effect on the bubble damping; however, the other terms, while independently having a smaller impact, do sum to have a net effect on the bubble that is worth considering.

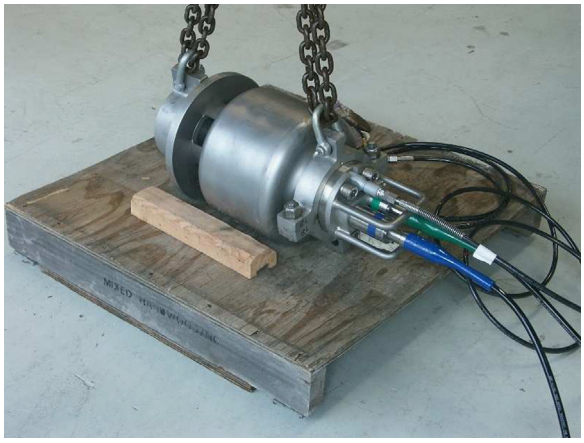


Fig. 9. The type 520 SERCEL airgun owned by DSTO.

4. Pressure field

According to Gilmore, the pressure and liquid velocity fields surrounding the bubble are given by

$$p_l - p_\infty = \rho_\infty\left(\frac{y}{r} - \frac{u^2}{2}\right) + \frac{\rho_\infty}{2c_\infty^2}\left(\frac{y}{r} - \frac{u^2}{2}\right)^2 \tag{16}$$

$$u_l = \frac{y}{c_\infty r} + \frac{K_3 y^2}{c_\infty^3 r^2}\left(1 - \frac{y}{c_\infty^2 r} + \frac{K_3^2 y^4}{2c_\infty^8 r^4}\right) \tag{17}$$

$$t = t_R + \left(\frac{r-R}{c_\infty}\right)\left(1 - \frac{\dot{R}R}{c_\infty r}\right) \tag{18}$$

$$y = R\left(H + \frac{\dot{R}^2}{2}\right) \tag{19}$$

$$K_3 = \frac{c_\infty^3 R^2 \dot{R}}{y^2}\left(1 - \frac{\dot{R}^2}{2c_\infty^2}\right) - \frac{c_\infty^2 R}{y}\left(1 - \frac{\dot{R}}{c_\infty}\right) \tag{20}$$

where p_l and u_l are the pressure and velocity of the liquid at a point r, t is the corresponding time co-ordinate to these values, t_R is the time at which the characteristic started at the bubble

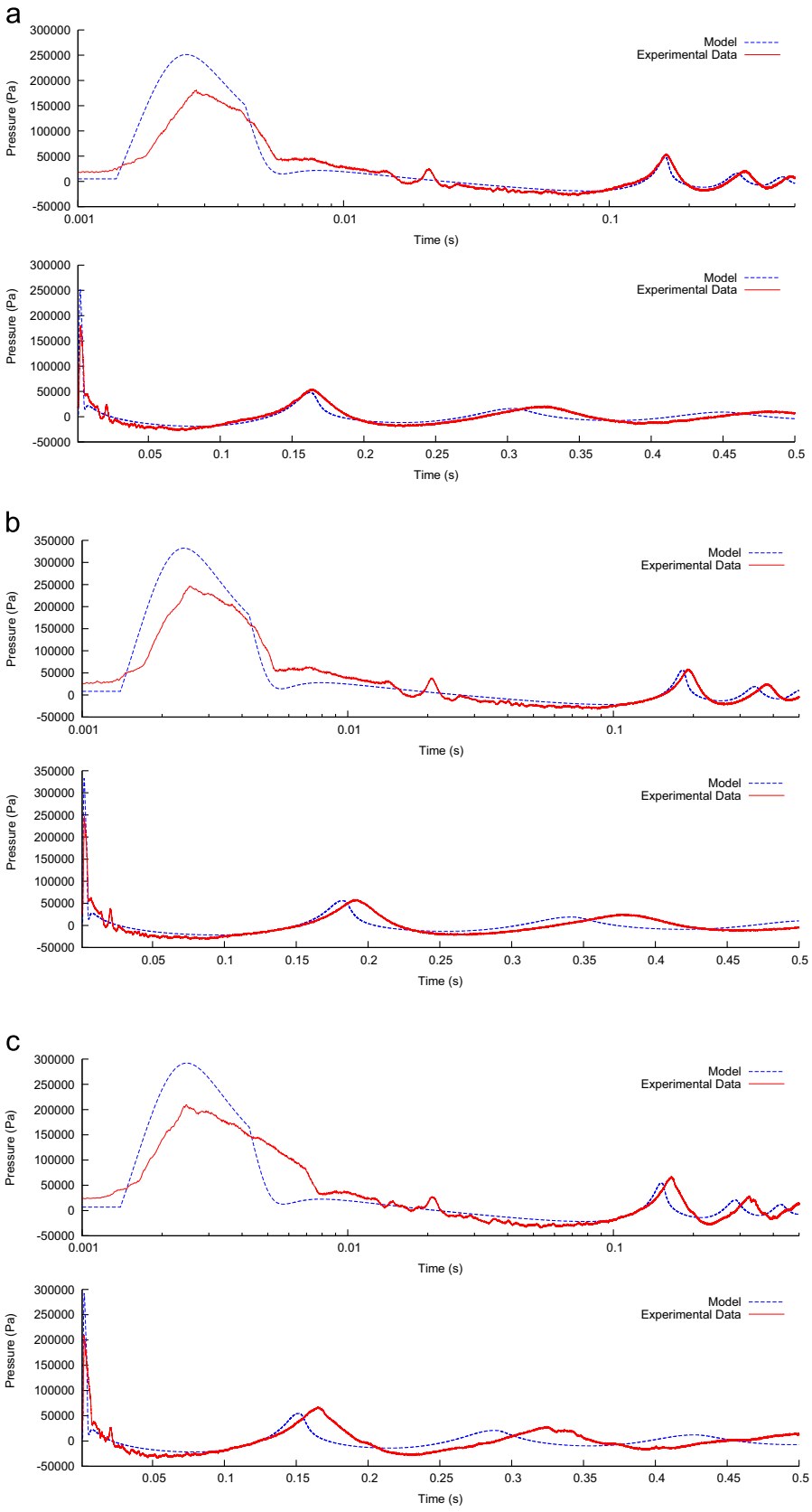


Fig. 10. Comparison of waveform produced by model with full scale experimental results: (a) Firing A, (b) Firing B and (c) Firing C.

wall ($r=R$) and y and K_3 are constants along any outgoing characteristic.

The reflection of the pressure waveform from the free surface is commonly known as the 'ghost' signal and it interacts negatively

with the direct pressure signal. The ghost signal is calculated using Eqs. (16)–(20), with r equal to r_g, given by

$$r_g = \sqrt{r_t^2 + (z_t + z_g)^2} \tag{21}$$

where r_t is the distance from the airgun to the pressure transducer, z_t is the depth of the transducer and z_g is the depth of the airgun.

5. Comparison of pressure–time history with experimental data

Free-field pressure measurements for single airgun firings have been measured by the Australian Defence Science and Technology Organisation (DSTO) (Corbishdale and Reid, 2010). The results were obtained with a SERCEL type 520 airgun (Fig. 9) in a test facility with a depth of approximately 15 m; airgun parameters for the bubble model are given in Table 1.

Fig. 10 compares the predicted pressure–time history of the current model (with κ=0.6 W/mK and a surface area magnification factor of 10 (Laws et al., 1990)) with the experimental results. The data is plotted on both log and linear scales to make evident the transient initial shock and period of the subsequent bubble pulsations, respectively. The specific trial parameters for each comparison are summarised in Table 2.

The small bump at approximately 0.02 s in the pressure waveforms of each of the firings is attributed to the reflection of the shock wave off the wall of the quarry in which the tests were performed (Corbishdale and Reid, 2010). The experiment was undertaken approximately 15 m from the wall. The time taken for the shock wave to reflect from the quarry wall corresponds with the timing of this additional pulse. A sharp reduction is evident in the pressure waveform at approximately 0.004 s for Firings A and B, and approximately 0.007 s for Firing C. These are attributed to the interference of the ghost signal with the direct signal (Corbishdale and Reid, 2010). The response of Firings A and B is measured at a depth of 3 m, and Firing C, at 5 m. The time at which the sharp reduction occurs is commensurate with the time it would take the shock wave to reflect from the surface and reach the pressure gauge. This sharp reduction is reproduced by the model through the inclusion of Eq. (21).

It is evident in Fig. 10 that there is some disparity between the modelled bubble period and the experimental data. For Firing A, the bubble period is approximately 4.5% under-predicted. The bubble period for Firings B and C is under-predicted by approximately 12%. SERCEL airguns release the firing air through four ports. It is possible that the initial four air jets do not merge to form one bubble but remain as four interacting bubbles. The period of multiple interacting bubbles increases when compared to a single bubble (Payne et al., 2005); however, the four bubbles are then each one quarter of the total volume and would have shorter periods. The interaction of the bubbles would need to lengthen the individual period by greater than 60–80%. The increased error in the bubble period of Firings B and C may be linked to the increased firing pressures. A larger surface area magnification factor for these bubbles due to higher turbulence (as a result of higher firing pressures) would increase heat transfer, lengthening the bubble period.

The magnitude of the initial shock is over-estimated by approximately 40%. The internal design of the airgun cause complicated flow passages and complexities to develop in the release of firing air. The limitations in modelling these phenomena and the resultant initial mass transfer significantly affect the prediction of the initial shock. No data is available for actual bubble size.

Comparison of the radius predicted by the present bubble model with experimental results will be the subject of future work. A scale model airgun and testing facility has been developed for controlled analysis of the bubble physics and pressure field.

Table 1
Parameters for the bubble model for the type 520 SERCEL airgun.

Firing air volume	8521 cm^3
Equivalent initial radius	0.12671 m
Airgun body volume	0.0270 m^3
Throttling area	0.0128 m^2, 0.0074 m^2[a]

[a] The first area is based on the port size; a reduced area was estimated due to overprediction of the initial shock magnitude.

Table 2
Configuration parameters for airgun firings.

Trial configuration	
Firing A	
Firing air pressure	138 bar
Airgun depth	3 m
Pressure gauge depth	3 m
Horizontal standoff	2.22 m
Firing B	
Firing air pressure	207 bar
Airgun depth	3 m
Pressure gauge depth	3 m
Horizontal standoff	2.22 m
Firing C	
Firing air pressure	172 bar
Airgun depth	5 m
Pressure gauge depth	5 m
Horizontal standoff	2.22 m

6. Conclusion

Various models have been studied that could account for differences in airgun bubble dynamics between theoretical predictions and experimental observations. From the present study, the most likely primary cause of additional damping to the seismic airgun bubble is heat transfer between the water and the air. This is potentially enhanced by an increase in bubble surface area due to turbulent motion near the bubble wall. The Gilmore pressure model has been used to predict the pressure waveform based on bubble motion calculated with the improved model. From comparison with experimental data, the increase in surface area is in the order of a factor of 10, which is in agreement with previous findings. Mass throttling as the air is released impacts the first maximum radius of the bubble and the magnitude of the initial shock wave significantly. The pressure waveform and bubble period results have been compared with experimental data with fair agreement. Further comparison of the model with experimental bubble radii measurements will assist in determining the reason for under-prediction of the bubble period and initial shock magnitude.

Acknowledgements

This work has been funded by the Maritime Platforms Division of the Defence Science and Technology Organisation (DSTO) and the authors wish to acknowledge the support of Dr Stuart Cannon and Mr Warren Reid.

References

Cook, J.A., Gleeson, A.M., Roberts, R.M., Rogers, R.L., 1997. A spark-generated bubble model with semi-empirical mass transport. J. Acoust. Soc. Am. 101 (4), 1908–1920.

Corbishdale, A., Reid, W., 2010. Air Gun Free Field Pressure Analysis. Technical Report DSTO-TR-2506. DSTO.

de Graaf, K., Penesis, I., Brandner, P., 2012. Comparison of the Rayleigh–Plesset and Gilmore equations and additional aspects for the modelling of seismic airgun bubble dynamics. In: 18th Australasian Fluid Mechanics Conference. Launceston, Australia.

Dragoset, W., 1984. A comprehensive method for evaluating the design of airguns and airgun arrays. In: Offshore Technology Conference. Houston, Texas, pp. 75–84.

Flynn, H.G., 1975. Cavitation dynamics. I. A mathematical formulation. J. Acoust. Soc. Am. 57 (6), 1379–1396.

Franc, J., Michel, J., 2004. Fundamentals of Cavitation. Kluwer Academic Publishers, Dordrecht, The Netherlands.

Fujikawa, S., Akamatsu, T., 1980. Effects of the non-equilibrium condensation of vapour on the pressure wave produced by the collapse of a bubble in a liquid. J. Fluid Mech. 97 (3), 481–512.

Gilmore, F., 1952. The Growth or Collapse of a Spherical Bubble in a Viscous Compressible Liquid. Technical Report No. 26-4. California Institute of Technology.

Herring, C., 1949. Theory of the pulsations of the gas bubble produced by an underwater explosion. In: Underwater Explosion Research: v. 2, 1950. Officer of Naval Research, Dept of the Navy.

Johnston, R.C., 1982. Development of more efficient airgun arrays: theory and experiment. Geophys. Prospect. 30 (6), 752–773.

Langhammer, J., Landrø, M., 1993. Temperature effects on airgun signatures. Geophys. Prospect. 41 (6), 737–750.

Laws, R.M., Hatton, L., Haartsen, M., 1990. Computer modelling of clustered airguns. First Break 8 (9), 331–338.

Li, G.F., Cao, M.Q., Chen, H.L., Ni, C.Z., 2010. Modeling air gun signatures in marine seismic exploration considering multiple physical factors. Appl. Geophys. 7 (2), 158–165.

Ni, C.Z., Chen, H.L., Liu, J., Ye, Y., Niu, H., Cao, M. Q., Liu, Y., 2011. Parameter optimization in air-gun type-dependent signature modelling. In: 73rd EAGE Conference & Exhibition incorporating SPE EUROPEC. Vienna, Austria.

Payne, E.M., Illesinghe, S.J., Ooi, A., Manasseh, R., 2005. Symmetric mode resonance of bubbles attached to a rigid boundary. J. Acoust. Soc. Am. 118 (5), 2841–2849.

Safar, M.H., 1976. Efficient design of airgun arrays. Geophys. Prospect. 24 (4), 773–787.

Schulze-Gattermann, R., 1972. Physical aspects of the airpulser as a seismic energy source. Geophys. Prospect. 20 (1), 155–192.

Vaage, S., Ursin, B., 1987. Computation of signatures of linear airgun arrays. Geophys. Prospect. 35 (3), 281–287.

Vokurka, K., 1986. Comparison of Rayleigh's, Herring's and Gilmore's models of gas bubbles. Acustica 59 (3), 214–219.

White, F., 2003. Fluid Mechanics, 5th edition McGraw Hill, New York, NY.

Ziolkowski, A., 1970. A method for calculating the output pressure waveform from an airgun. Geophys. J. R. Astron. Soc. 21, 137–161.

Ziolkowski, A., 1982. An airgun model which includes heat-transfer and bubble interactions. In: SEG Annual Meeting. Dallas, Texas, pp. 187–189.